Digital Illumination in Microscale Direct-Writing Photolithography: Challenges and Trade-Offs

1st Mark Stonehouse
Institute of Photonics
Department of Physics
University of Strathclyde
Glasgow, Scotland, UK
mark.stonehouse@strath.ac.uk

2nd Yanchao Zhang
Information Optoelectronics Research Institute
Harbin Institute of Technology at Weihai
Weihai, 264209, China
zhangyanchao66@sina.com

3rd Benoit Guilhabert
Institute of Photonics
Department of Physics
University of Strathclyde
Glasgow, Scotland, UK
benoit.guilhabert@strath.ac.uk

4th Ian Watson
Institute of Photonics
Department of Physics
University of Strathclyde
Glasgow, Scotland, UK
i.m.watson@strath.ac.uk

5th Erdan Gu
Institute of Photonics
Department of Physics
University of Strathclyde
Glasgow, Scotland, UK
erdan.gu@strath.ac.uk

6th Johannes Herrnsdorf
Institute of Photonics
Department of Physics
University of Strathclyde
Glasgow, Scotland, UK
johannes.herrnsdorf@strath.ac.uk

7th Martin Dawson
Institute of Photonics
Department of Physics
University of Strathclyde
Glasgow, Scotland, UK
m.dawson@strath.ac.uk

***Abstract*—We explore the adaptation of existing photolithography technologies and introduce the potential for additional functionality in the form of structured light. By using a complementary metal oxide semiconductor (CMOS) controlled micropixellated light emitting diode (LED) array, features such as object recognition, tracking and characterization are possible in combination with photo-curing. We discuss the observed trade off between the delivered power density and resolution capability of the system due to the requirements of the additional features.**

I. Introduction

So-called digital illumination is the concept of modulating an illumination source with a digital signal. Important examples are light-fidelity and visible light positioning [1], [2]. Another emerging form of digital illumination is structured illumination, which has been applied to visible light positioning [3], [4] and microscopy [5]. The emergence of these capabilities allows for multipurpose systems, which are capable of finding and tracking a specified object and communicating with it.

Here, we describe an experimental setup that will allow us to use structured illumination in the context of micro fabrication via maskless lithography. Maskless photolithography hosts many benefits over conventional lithography due to not requiring a quartz mask, which is both time consuming and expensive to manufacture. Several such techniques have been developed including interference lithography, 2-photon writing and direct writing using both LEDs and lasers [6]–[9]. Modern LEDs are not only able to emit light at wavelengths comparable to mercury lamps, e.g. 365 nm and 405 nm for i-line and h-line respectively, but III-nitride LEDs are being developed which are able to emit in the deep UV wavelengths, approximately 240-280 nm, which is more suitable for common photo-acid generators used for photopolymerisation. In the work we report here, a CMOS interface to a micro LED (μLED) array is capable of illuminating the sample with a time-sequence of illumination patterns, which can be used directly for photo-curing or for auxiliary functions such as positioning and alignment. The sample is mounted on a motorized XYZ stage, which is controlled through the same interface as the LED array thus allowing coordination of the structured illumination with the sample motion.

In this report, we focus on the design considerations of a direct writing setup that employs structured illumination. Single LEDs within an array have been successfully applied to maskless lithography in similar direct writing setups [8], [10]. However, there were some limitations, which needed to be overcome in order to incorporate the desired new functionality. This was due to the use of a microscope objective lens only having a sufficient field of view (FOV) to image a 4×4 subsection of the array, therefore severely limiting the capability of using structured illumination techniques. In order to rectify this, we replaced the objective lens with an aspheric lens to collect and collimate the light and a beam expander to alter the demagnification. With this setup we were able to utilize a 16×16 array with projected a light spot size of 20 μm and a polymerized feature size of ≈40-45 μm diameter.

II. LED Array Used

The device employed here is a 16×16 pixel array of individually addressable 405 nm-emitting μLEDs flip-chip bonded onto a custom CMOS control chip [11]. Each LED is 72 μm in diameter, spaced on a 100 μm center-to-center pitch, and

All work was funded through EPSRC under grant no. EP/P02744X/2. Also thanks to Ruaridh Winstanley and John McPhillimy for their help in the characterization of the cured materials. Data available at http://dx.doi.org/10.15129/9b7c92b3-f7ac-4be7-b0b5-ba31ac30c35c

the original epitaxial structure was grown on c-plane sapphire. The pixel size is limited by the gold bump bonding (50 μm minimum), though this could be reduced to 10 μm through indium bonding. In direct current (DC) operation we measured the typical average power of a single emitting pixel to be 15.3 μW at a driving current density of 1950 A/cm^2, though performance varied throughout the array. This characteristic is illustrated in Fig. 1, which also shows that the variation is most pronounced among the outer pixels.

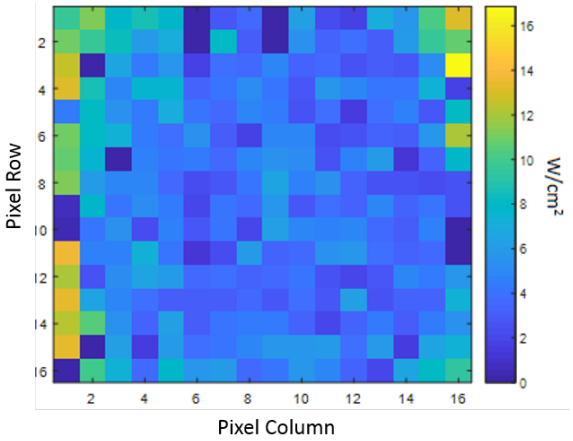

Figure 1. A 'heatmap' of the 16×16 pixel LED array showing the variations in power density about an average of 4.87 W/cm^2 at 1950 A/cm^2.

Detailed electrical and optical characteristics of comparable devices have been documented previously [12]. The 405 nm device has a -3dB modulation bandwidth over 100 MHz [12], which is well above the maximum rate here at which the CMOS control chip can load 'patterns' from an field-programmable gate array (FPGA) driver (XEM3010-1000 from Opal Kelly). Control is via a MATLAB script in which we are able to define 'patterns', which dictate which LEDs become active and sequentially modulate the array with them. The modulation rate is limited to 2000 Hz, though the exposure dose may be decreased through the use of pulse-width modulation and reducing the duty cycle of each pattern.

III. System Architecture

A schematic and photograph of the photolithography setup is shown in Figure 2. Here we see the LED array and associated CMOS and FPGA drivers mounted horizontally on a manual XYZ stage. The light is then collected and collimated with an aspheric lens and added into the main optical path with a dichroic mirror (with 450 nm wavelength cutoff). The beam is then passed through two spherical lenses to magnify the projected patterns to match the FOV we require before reflecting off a second dichroic mirror (with 425 nm wavelength cutoff) and focused through a vertical infinity-corrected objective lens (Thorlabs RMS10X). The resultant optical spot diameter is ≈20 μm. The sample is mounted onto a right-angle bracket attached to a motorized XYZ stage (Newport 9064-XYZ-PPP) to allow automated movement in coordination with the structured light pattern. The pattern is imaged with a CCD camera (FLIR CM3-U3-13Y3C) mounted above the second dichroic mirror using an infinity-corrected tube lens to control its FOV.

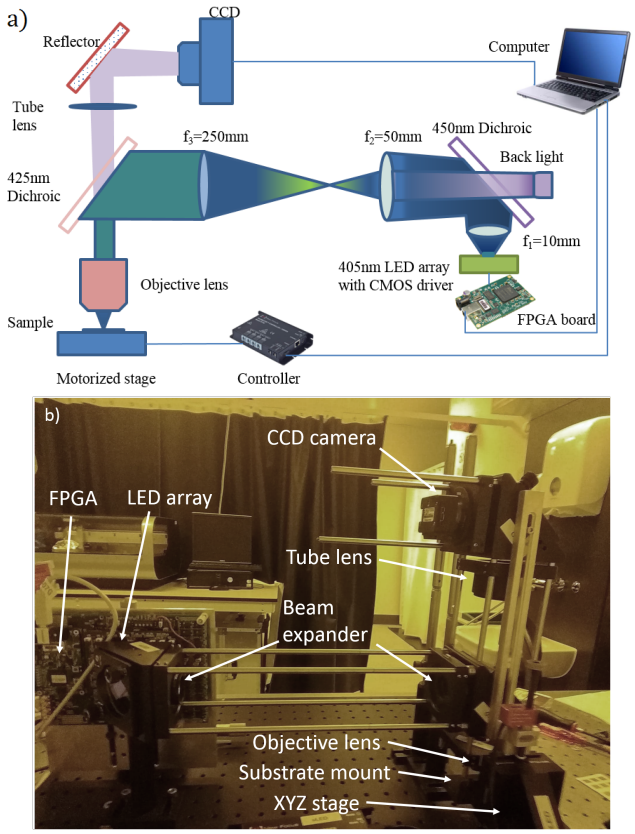

Figure 2. a) A schematic of the photolithgraphy system. b) A photograph of the system.

The motorized XYZ stage is capable of a 0.5 μm resolution which allows for the accurate focusing and XY movement of the substrate, thus allowing for continuous microstructures to be fabricated. The driver electronics (Newport 8742-4) are able to move the stage at a maximum rate of 1 mm/s whilst maintaining its 0.5 μm resolution. The combination of a 16×16 LED array and the stage's 25 mm×25 mm movement range, allows for up to 20,700 separate exposure patterns without changing or remounting the substrate. The camera is able to resolve 2 μm features over a 2.56 mm×2 mm area which is adequate for the feature sizes being produced. Both the motorized stage and the LED array are capable of being driven simultaneously with the same MATLAB script allowing for automated control over both the exposure pattern/dose and the area of substrate exposed. This allows for large areas to be accurately patterned, either to produce large custom microstructures or to mass produce smaller ones. Additionally, the integrated control allows for any information which can be collected in real time to be also analyzed and acted upon live. Beyond sequential image capture of microstructures under fabrication, self-alignment and feature tracking functions can

be incorporated. In order to successfully implement any form of structured light functionality, a reasonable FOV is required. Because of this, a trade-off is created between having a low enough demagnification to allow for this addition, while still requiring a small projected spot size to give a reasonable feature resolution and high enough power density to cure the photo-resist in reasonable times.

IV. System characterization

There is an average projected optical power per pixel of 15.3 μW at a DC drive current density of 1950 A/cm^2, and variations between pixels, have been noted in Section II. These variations could be due to degradation from previous use, variations in local heat dissipation, or other non-uniformity arising from the original device fabrication. The spot size of $\approx$20 μm was derived from projecting spots from multiple LEDs onto a printed grid of known line width and separation. Additionally, intensity profiles were measured across perpendicular axes as shown in Fig. 3 and FWHM values were derived. The spots are shown to be reasonably uniform in both shape and power density. Also, due to the inherent top hat shape of the emission profile, the FWHM of 17 μm is similar to the total spot size. This intensity profile is superior compared to a Gaussian as it should give well defined feature edges in photolithography.

When calculating the power density, the beam was considered to be uniform. This gives a power density of 6.74 W/cm^2 at half maximum position, which is able to provide a typical curing dose of 400 mJ/cm^2 in 59 ms. Loss mechanisms are now considered. Whilst the transmission losses are low, there are significant losses particularly in the initial light capture with the aspheric lens and in the beam expander. This divergence angle introduced at each stage can be calculated with Eq. 1.

$$\text{Divergence Angle} = 2arcsin(\frac{\eta_{air}}{\eta_{air}}\frac{l}{2d}) \quad (1)$$

Where the refractive indices are assumed to be air on each side of each lens, l is the diameter of the emitter and d is the distance between lenses. The initial divergence angle from the LED is 120°. An example is between the spherical lenses in the beam expander where we see a divergence of 8° which escalates to a optical power loss of $\approx$89%. With the 60 mm cage system chosen for practicality and adaptability, we are approaching the practical limit of what is achievable in terms of increasing the collection efficiency. This loss is also unavoidable as the need for an adequate FOV, and therefore additional optics, far outweighs the need for a higher power density.

V. Patterning and results

To test the system, we used a commercially available UV resin (from ANYCUBIC) designed for 3D printing and that cures at 405 nm. This acts as a negative photo-resist and is able to be spin coated to 5-10 μm thickness, allowing a good lateral feature resolution. Another benefit of the resin is its good adhesion to glass allowing for borosilicate glass to be used as a substrate. Glass cover slips were cleaned in an ultrasonic bath with acetone followed by methanol. Subsequently they were rinsed in deionized (DI) water and baked on a hotplate at 110°C for 25 minutes. The resin was then spin coated at 3200 rpm for 20 s. This gives a 9 μm film thickness, as measured on a stylus profilometer (DekTak). The sample was then transferred to the lithography system and exposed for 27 ms seconds giving an estimated dose of 181 mJ/cm^2. The sample was then immediately submerged and gently moved in toluene for 10 s before being rinsed in DI water. Fig. 4 shows results of a projection of an example pattern using 19 pixels chosen to be power matched within $\pm$1 μW under test conditions previously specified. These pixels also have minimum separations twice the array pitch to help assess the pattern resolution achievable in the polymerized resist. To provide a distinctive orientation and marker feature, a further 3$\times$3 group of LEDs in a corner of the array were also illuminated, and this group included one low-power pixel. Fig. 4 b) shows that each of the 19 non-adjacent pixels generated a discrete polymerized spot, although considerable distortion of the pattern and individual feature shapes occurred, probably owing to non-optimized current processing. The resolution of individual spots was lost, however, in the feature produced by illumination of the cluster of adjacent pixels.

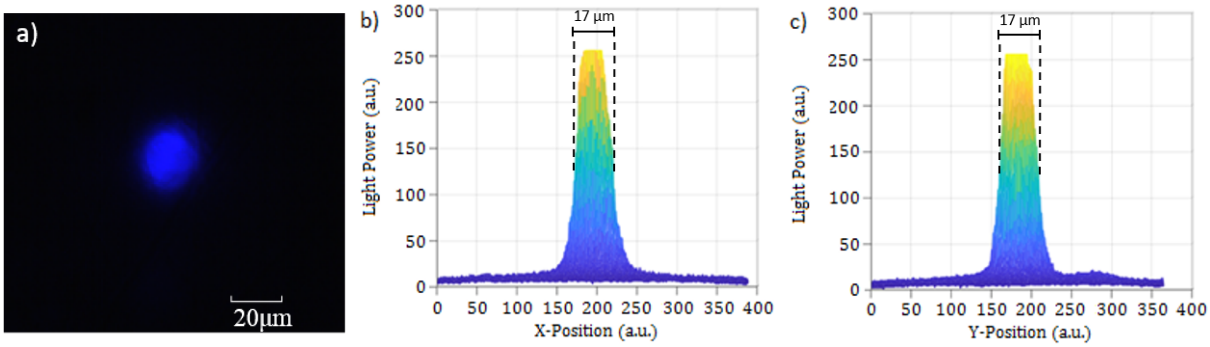

Figure 3. a) Optical image of a single projected spot. b) The x-axis intensity profile of the same spot. c) the y-axis intensity profile of the spot.

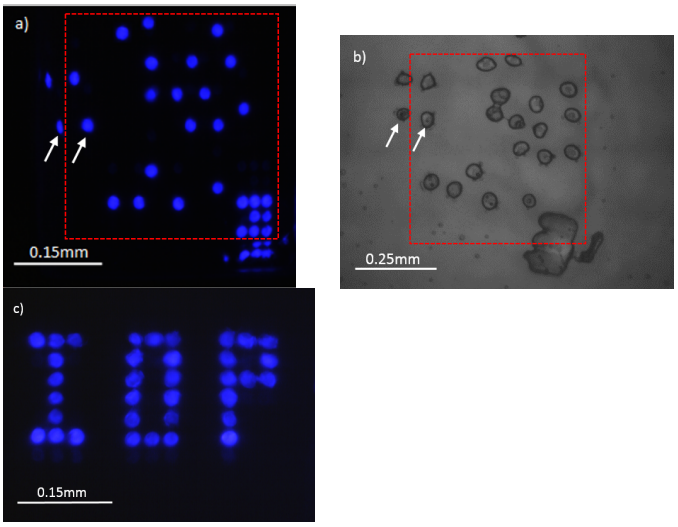

Figure 4. a) Optical image showing the multiple spots produced by an example illumination pattern. The red dotted overlay frame shows the perimeter of the array, and arrows indicating an example of peripheral spots and their reflection outside the frame b) Optical image of the cured resist pattern with similar annotation. The polymerized dots are seen to be ≈40-45 μm wide and 5 μm high. c) A projected pattern of the 'Institute of Photonics' logo to demonstrate the selective pattern capabilities.

Fig. 4 also illustrates artifacts which arise with the flip-chip LED array used here. The packaging produces reflections from the outer two rows of pixels, which are in the same focal plane as the actual LEDs. Therefore, in curing tests these reflections are able to produce additional unwanted features as highlighted in Fig. 4, and affecting two non-adjacent pixels in the main pattern as well as the cluster of pixels used as a marker. As this behavior is inherent to the device itself and new versions are being fabricated to reduce this effect.

VI. Conclusions

We have produced a mask-less photolithography system capable of not only producing micrometer scale features, but which also offers the flexibility to incorporate additional layers of functionality in the form of structured light, and optional addition of a second LED array. The current system is capable of simultaneously exposing a 16×16 digital pattern producing ≈40-45 μm features in a resist material. Due to the adaptability of the setup this may be easily changed by either swapping the LED array or by changing the beam expander. Furthermore, owing to the integrated CMOS drive scheme, it is capable of precisely controlling the projected patterns and the exposure. These results show the strengths of μLED based photolithography for easy and efficient fabrication of large-area or repeated designs through precise array and stage control. The FOV has been chosen to still provide a reasonable power density at the sample whilst collecting output of the entire LED array. A further design consideration was that the beam expander was chosen to provide an appropriate scaling for potential use of multiple LED arrays which negates for the need for additional optics when incorporating structured light elements. The associated power losses are justified by the need for a suitable FOV at the sample and these losses would be seen at the objective lens regardless.

References

[1] T. Komine and M. Nakagawa. "Fundamental analysis for visible-light communication system using LED lights". In: *IEEE transactions on Consumer Electronics* 50.1 (2004), pp. 100–107.

[2] T. Do and M. Yoo. "An in-depth survey of visible light communication based positioning systems". In: *Sensors* 16.5 (2016), p. 678.

[3] J. Herrnsdorf, M. J. Strain, E. Gu, et al. "Positioning and space-division multiple access enabled by structured illumination with light-emitting diodes". In: *Journal of Lightwave Technology* 35.12 (2017), pp. 2339–2345.

[4] J. Herrnsdorf, M. D. Dawson, and M. J. Strain. "Positioning and Data Broadcasting using Illumination Pattern Sequences Displayed by LED Arrays". In: *IEEE Transactions on Communications* (2018).

[5] N. Radwell, K. J. Mitchell, G. M. Gibson, et al. "Single-pixel infrared and visible microscope". In: *Optica* 1.5 (2014), pp. 285–289.

[6] I. Byun and J. Kim. "Cost-effective laser interference lithography using a 405 nm AlInGaN semiconductor laser". In: *Journal of Micromechanics and Microengineering* 20.5 (2010), p. 055024.

[7] J. Serbin, A. Egbert, A. Ostendorf, et al. "Femtosecond laser-induced two-photon polymerization of inorganic–organic hybrid materials for applications in photonics". In: *Optics letters* 28.5 (2003), pp. 301–303.

[8] B. Guilhabert, D. Massoubre, E. Richardson, et al. "Sub-micron lithography using InGaN micro-LEDs: mask-free fabrication of LED arrays". In: *IEEE Photonics Technology Letters* 24.21 (2012), p. 2221.

[9] C. Rensch, S. Hell, M. v. Schickfus, et al. "Laser scanner for direct writing lithography". In: *Applied optics* 28.17 (1989), pp. 3754–3758.

[10] D. Elfström, B. Guilhabert, J.J.D. McKendry, et al. "Mask-less ultraviolet photolithography based on CMOS-driven micro-pixel light emitting diodes". In: *Optics Express* 17.26 (2009), pp. 23522–23529.

[11] H. X. Zhang, D. Massoubre, J.J.D. McKendry, et al. "Individually-addressable flip-chip AlInGaN micropixelated light emitting diode arrays with high continuous and nanosecond output power". In: *Optics express* 16.13 (2008), pp. 9918–9926.

[12] J.J.D. McKendry, R. P. Green, A. E. Kelly, et al. "High-speed visible light communications using individual pixels in a micro light-emitting diode array". In: *IEEE Photonics Technology Letters* 22.18 (2010), pp. 1346–1348.